ROTOR WAKE AND INFLOW CHARACTERISTICS OF MULTIROTOR DRONE CONFIGURATIONS

Po-Wei Chen, aewebberchen@gatech.edu, Georgia Institute of Technology (USA)

Dhwanil Shukla, dhwanil.shukla@gatech.edu, Georgia Institute of Technology (USA)

Lakshmi Sankar, lsankar@ae.gatech.edu, Georgia Institute of Technology (USA)

Narayanan Komerath, komerath@gatech.edu, Georgia Institute of Technology (USA)

JVR Prasad, jvr.prasad@ae.gatech.edu, Georgia Institute of Technology (USA)

Abstract
A coordinated experimental and computational study of multirotor configurations has been carried out at low Reynolds numbers. The configurations include coaxial rotors, horizontally spaced side-by-side rotors, and tandem rotors separated by horizontal and vertical spacing, both. The calculations have been done at a nominal total thrust coefficient of 0.008. Although rotor performance, tip vortex trajectories, and flow velocity distributions are all of interest, the present study has focused on the inflow velocity field at a number of planes immediately above and below the rotor disks, for the express purpose of developing reduced order inflow models. Test data and the computations for the time averaged inflow and outflow fields compare well with each other. Significant rotor-wake interaction phenomena are seen due to the close proximity of the rotor disk, even when the rotors are in hover. Dynamic inflow coefficients have been extracted for representative strong rotor-vortex interaction scenarios.

1. INTRODUCTION

There has been a large body of work on wake characteristics and inflow flow field characteristics of large scale rotors. Experimental and computational data are available for single and coaxial rotors, and for tandem rotor configurations Ref. 1-12. Results are available for rotor performance in hover and forward flight, spanwise and azimuthal blade loading, and wake structures. These results are being used to improve dynamic inflow models and comprehensive aeroelastic analyses.

A similar set of data is not available for small scale rotors that are in use in drones and other autonomous systems [Ref. 13-19]. The small rotor radius, combined with small chord, imply low Reynolds numbers. The aerodynamic characteristics of the blade sections at such Reynolds numbers differ significantly from conventional rotors at higher Reynolds numbers. Both the static and dynamic stall characteristics are widely different. The wake trajectories are also different both due to the increased diffusion at lower Reynolds numbers and the differences in the descent and contraction rates compared to large scale rotors. Interaction between closely spaced rotors in coaxial, tandem, or quadrotor configurations cause further complications. Work is

urgently needed to characterize these effects through complementary experimental and computational studies, in order to develop reliable inflow models for use in flight dynamics simulations.

The present work is motivated by this need for developing a good understanding of the inflow characteristics of multirotor configurations. The following approach is used:

1. A series of experimental studies are done for single, coaxial and tandem rotor configurations at low Reynolds numbers in hover. Detailed measurements of the inflow velocity field and visualization of the wake structures are done.

2. Guided by these experimental studies, computational fluid dynamics simulations are performed for the same configurations at low and high Reynolds numbers to determine how Reynolds number effects affect the performance (thrust vs. power), radial and azimuthal airloads, wake structure, and inflow at the rotor disk.

3. The First three components of the dynamic inflow velocity (mean flow, longitudinal, and lateral variations) are extracted to assess how the spacing between adjacent rotors and the differences in Reynolds number (between large and small-scale rotors) affect the inflow.

2. EXPERIMENTAL SET-UP

The hover experiments were conducted in the 2.13m × 2.74m (7 ft × 9 ft) test section of the John Harper closed circuit low speed wind tunnel at the Georgia Institute of Technology [Ref. 20-23]. The upper rotor is suspended from the ceiling and the lower rotor is supported from the floor such that the rotors are approximately 1.5 meters above the floor. The support rods were in-line with the rotor axes to avoid their interaction with the rotor inflow and wake.

The horizontal and vertical spacing between the two rotors may be changed to study a wide range of rotor configurations of interest. The rotors are powered by brushless DC motors (BLDC). The upper rotor rotates counter clockwise and the lower rotor clockwise. The collective pitch on both rotors may be adjusted independently during the test runs through variable pitch assemblies actuated using servos. The rotor speeds are monitored and controlled within +/- 10 RPM of the set values using laser tachometers and a microcontroller that employs a proportional feedback loop control. The thrust and torque generated by the rotors are measured independently using load cells.

For the torque measurements, the motor mounts are mounted on the support rods through friction-less bearings. The rotation about the bearings is restricted by 0.1 kgf range load cells placed off-centre such that the counter torque necessary to keep the motor mount from rotating about the bearing due to aerodynamic torque is provided through them. Thrust is measured using 1kgf range load cell placed along the rotor axis.

Signals of all the load cells are passed through low-pass filters set at 40 Hz and amplified before reading them using data acquisition device (DAQ). The thrust and the torque data has been collected at the rate of 1000 Hz for a span of 60 seconds and then averaged. Figure 1 shows the setup for a typical coaxial rotor configuration.

High-speed stereo particle image velocimetry (SPIV) has been used to quantify the inflow velocity distributions and for tracking the streamlines through the rotors. SPIV captured the flow field on a vertical plane in the region between the two rotors.
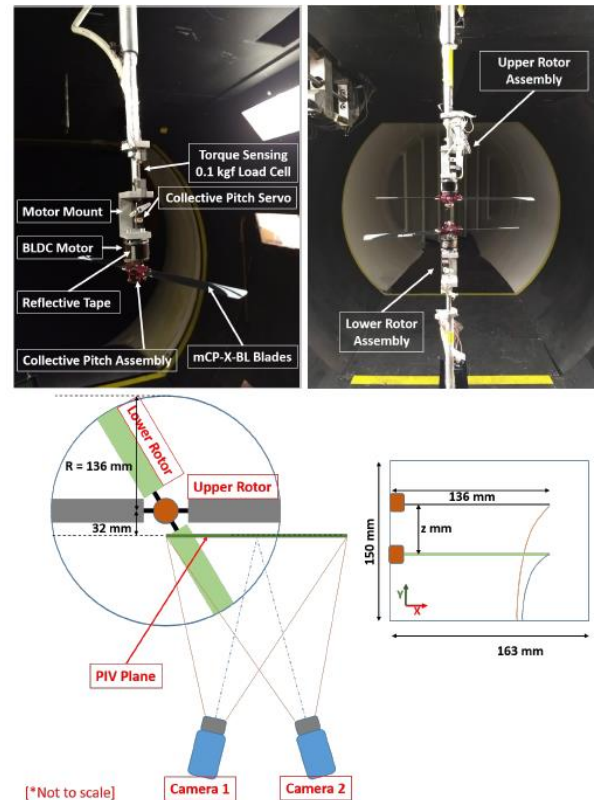

Figure 1. Experiment setup for the coaxial rotor

3. COMPUTATIONAL METHODOLOGY

An in-house solver named GT-Hybrid has been used, the schematic view of the hybrid method is shown in Figure 2. GT-Hybrid employs a hybrid wake methodology, meaning that the flow field is only resolved within a small structured grid domain surrounding a single reference rotor blade. Within this grid, the discretized from of Navier-Stokes equations are solved using a third order accurate flux-limited monotone upwind scalar conservation law (MUSCL) scheme. A fully implicit first order accurate temporal marching scheme has been used. Outside of this small gridded domain, the self-generated wake as well as the wake from other blades is efficiently modelled with a grid-free field of vorticity elements. The loading and the flow field on the other blades are assumed to lag the current blade. The flow is assumed to be laminar, since the Reynolds number based on the tip speed and the tip chord is around 80,000.

All the simulations in this study were analysed after 10 rotor revolutions to eliminate impulsive start effects. The wake generated by each rotor blade is modeled as 15 trailers, and resolved for 15 revolutions of wake age. Because the bound circulation over the rotor varies with time, shed wake filaments are generated once every 5 degrees of azimuth.
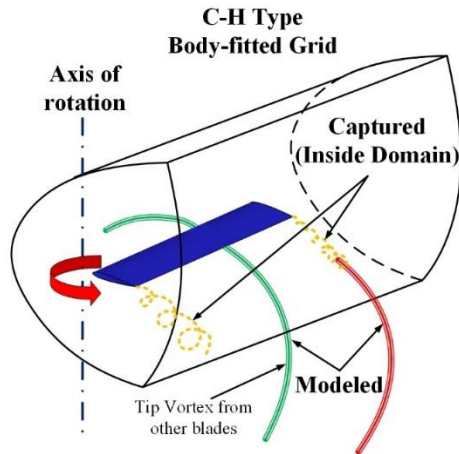
Figure 2. Schematic View of the Hybrid Method

4. ROTOR CONFIGURATIONS

A two bladed untwisted rotor with a rectangular planform, made of NACA 0010 airfoil sections, has been studied in the present work. The rotor characteristics are given below in Table 1.

Table 1. Rotor Geometry and Characteristics

Rotor Characteristic	
Number of rotors, b	2
Number of blades	2 blades per rotor
Chord length, c	0.019m (0.062 ft.)
Rotor radius (R)	0.136m (0.446 ft.)
Solidity $bc/(\pi R)$	0.0890
Root cutout radius	0.021m (0.069 ft.)
Tip speed	61.5 m/s (201.8 ft./s)
Tip Reynolds Number	80,000

In the experimental set up, the axial spacing (AS) and vertical spacing (VS) between the two rotors may be readily varied to model coaxial and tandem rotor configurations as shown in Figure 3.
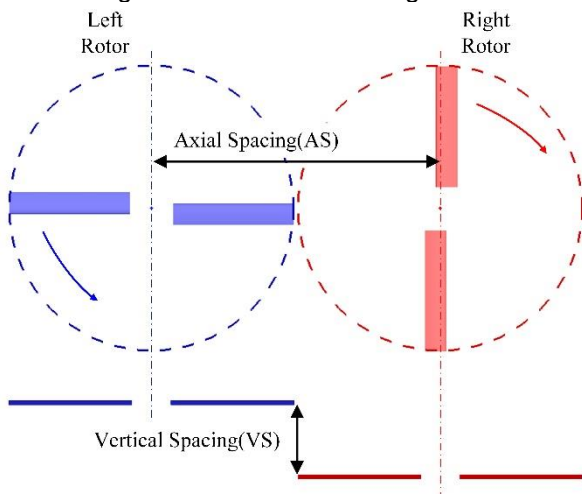

Figure 3. Rotor configuration

Table 2 below gives details of the configurations that have been analysed experimentally and computationally.

Table 2. Rotor Configurations

Rotor Configuration	Axial Separation (AS)	Vertical Separation (VS)
Coaxial Rotor	0	0.25R/0.40R
Side-by-Side Rotor	2.1R/2.2R/ 2.3R/2.4R	0
Tandem Rotor	0.25R/0.5R/ 0.75R/1.0R/ 1.25R/1.5R	0.25R/0.40R

The rotor separation of 0.25R and 0.40R shown in Table 2 was chosen based on the range of rotor separations found in commercially available coaxial rotor UAVs such as HAK303, HAK787, Sprite™, and WorkFly™. For a complete experimental study of these configurations, the reader is referred to Ref. 22.

5. RESULTS AND DISCUSSION

The available test data included rotor performance (thrust vs. power), tip vortex trajectories, and PIV data. The primary focus of the computational studies is the development of inflow models that may be used in helicopter and UAV/drone flight dynamics simulations. For this reason, much of the comparisons in this section are limited to velocity field comparisons. Prior work on rotor performance and wake trajectories may be found in Ref. 24 and 25.

The total thrust coefficient C_T of the two-rotor setup was kept constant at 0.008 for all cases. The rotors were trimmed in the experiments until the total target thrust was met and the rotor torques equalized. The calculations directly used the collective pitch sittings from the experiment, without additional trim.

5.1. Coaxial Rotor

The hi-speed PIV was performed on a plane 32 mm offset from the rotor centre to avoid motor mount shadows. Given that the rotor wake is symmetric in hover, data was collected only over the right half of the rotor setup as shown in Figure 1.

Figure 4 shows the rotor inflow for the coaxial rotor at a vertical spacing of 0.25 R. The inflow and outflow data presented here are extracted at a distance 0.1 R above and below the rotors respectively for both the rotors.

The velocity field above the upper rotor is smooth as expected. The comparisons between the test data and the simulations are in very good agreement. At the plane just below the upper rotor, the outflow (axial) velocity distribution linearly varies from the root cut-out to 80%R. The hybrid method used in this study predicted a more rapid contraction of the tip vortex structure from the upper rotor compared to test data. The velocity gradient outboard of the tip vortex trajectory was captured in magnitude and slope, although there was 0.05 R difference in the tip vortex trajectory radial position passing through the measurement plane. This difference is likely due to the vortex line representation of the tip vortex and inner wake, with an assumed vortex core. Small changes to these parameters can dramatically change the velocity field in the immediate vicinity of the strong tip vortex structure, influencing its radial contraction and axial descent rate, both.

The predicted inflow through the lower rotor compares well with the measurements, except in the immediate vicinity of the tip vortex passage. The outflow below the lower rotor was under predicted in the calculations compared to test data, although other features such as the velocity jumps near the tip vortices from the top and bottom rotors were reasonably well resolved.
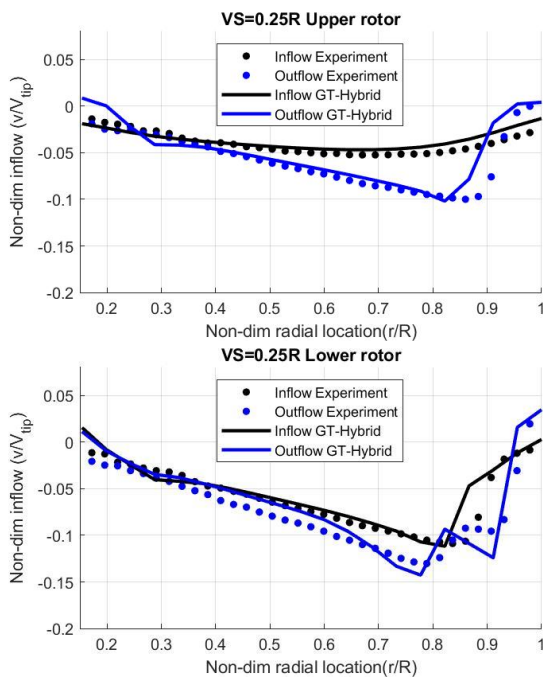

Figure 4. Inflow and outflow velocity profiles comparison for the coaxial rotor with VS=0.25R

5.2.   Side-by-side Rotor in Hover

This case is of interest, since many drone configurations are compact, and the rotors are placed very close to each other. Again, the total thrust coefficient was trimmed to 0.008 in the experiments, with zero net torque. The measured collective pitch was used to perform the simulations.
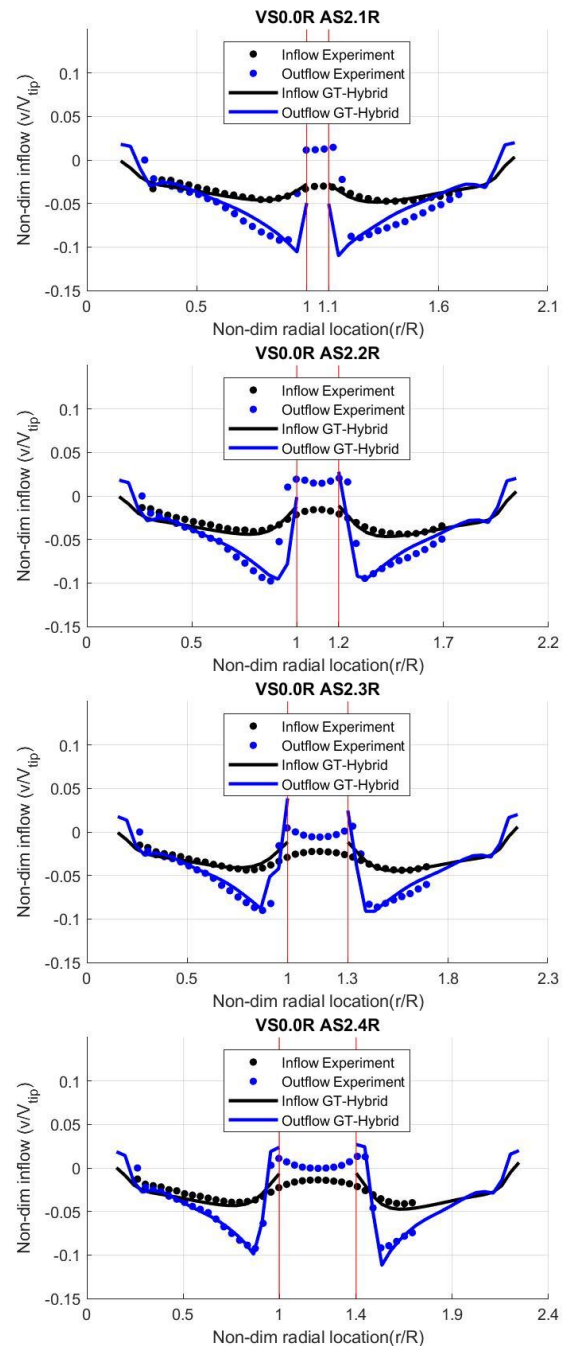

Figure 5. Inflow and outflow velocity profiles comparison for the side-by-side rotor with AS=2.1/2.2/2.3/2.4R

In Figure 5, the inflow and outflow velocity fields are shown for four representative axial spacing, ranging from 2.1R to 2.4 R. The comparisons between the text data and measurement are, in general, very good.

The inflow and outflow profile plots in Figure 5 contain some common features. Outflow profiles underneath both rotors are wedge-shaped with a linear increase in the magnitude of velocity as r varies from hub to tip, before dropping back to zero steeply just before the tip. Such a linear variation is common for simple untwisted rotors of rectangular planform. The peak in the outflow velocity profile consistently occurs near 90%R.

5.3. Tandem Rotor

The tandem rotor SPIV and performance tests were conducted at two vertical separations, and a range of axis shifts (AS) as listed in Table 2.

The time-averaged flow fields were computed using 200 instantaneous PIV frames. The average velocity fields were found to be within 2% of those obtained using 150 frames and within 0.5% of those obtained using 175 frames for all cases.

Figures 6-9 show comparisons of the computations with time averaged PIV data. The agreement is very good except in the immediate vicinity of the vortex blade interactions. The inflow and outflow data presented here are extracted on planes that are 0.1R above and below the rotors, respectively, for both rotors.

6. DYNAMIC INFLOW MODELS

The previous comparisons between the measurements and predictions were all made at a single azimuthal location (ψ=0 degree for the front rotor and 180 degrees for the aft rotor). The numerical calculations give velocity field over the over the entire rotor disk as shown in Figures 10-13. It is seen that the inflow distribution is highly three dimensional and unsteady. An actuator disk model that assumes that the inflow is axisymmetric and uniform would yield inaccurate results in flight dynamics simulations of the drone.

The CFD simulations shown in the previous are functions of non-dimensional radial ($\vec{r}$) and azimuthal locations(ψ). They are not directly useful in flight simulations, which rely on efficient dynamic inflow models for rapid, real-time simulations. The following methodology based on Ref. 26 is being used to reduce the data from the CFD results.

The induced velocity $\vec{v_z}(\vec{r}, \psi)$ at the rotor disk, normalized by the tip speed, is related to the mean thrust, and the rolling and pitching moments generated by the rotor at the hub. We may view the induced velocity as series in terms of the non-dimensional radial location ($\vec{r}$) and the azimuthal location (ψ). The first few terms of this series are:

$$\vec{v_z}(\vec{r}, \psi) = \lambda_0 + \lambda_{1c}\vec{r}\cos(\psi) + \lambda_{1s}\vec{r}\sin(\psi)$$

Once the induced velocity is available from experimental CFD simulations, we may compute λ_0, λ_{1c} and λ_{1s} as:

$$\lambda_0 = \frac{1}{\pi}\int_0^{2\pi}\int_0^1 \vec{v_z}(\vec{r}, \psi)\vec{r}d\vec{r}d\psi$$

$$\lambda_{1c} = \frac{4}{\pi}\int_0^{2\pi}\int_0^1 \vec{v_z}(\vec{r}, \psi)\vec{r}^2\cos(\psi)d\vec{r}d\psi$$

$$\lambda_{1s} = \frac{4}{\pi}\int_0^{2\pi}\int_0^1 \vec{v_z}(\vec{r}, \psi)\vec{r}^2\sin(\psi)d\vec{r}d\psi$$

Figures 14 and 15 show the extracted λ_0, λ_{1c} and λ_{1s} as a function of the axial spacing, at a vertical spacing VS of 0.25R and 0.40 R, respectively. For the left rotor, it is seen that the time averaged quantity λ_0 decreases slowly with increased axial spacing. For the right rotor, initially varies rapidly with the axial spacing due to the interaction of the left rotor wake with the right rotor disk. As the axial separation increases beyond 0.5R, λ_0 becomes less sensitive to axial separation. As may be expected, the rotor on the right, which operates partially in the outflow of the left rotor experiences higher λ_0. This, in practice, would translate into higher power consumption for ther right rotor compared to the left. The coefficient λ_0 for the two rotors will be expected to approach each other as the axial separation AS as a fraction of the rotor radius R goes to infinity.

It is also seen that λ_{1s} is nearly zero, indicating that inflow through the left and right rotors experiences very little lateral asymmetry for all the cases considered.

As may be expected, there is significant fore and aft asymmetry, and λ_{1c} is nonzero. The aft rotor experiences an upward directed flow (upwash) rather than a downwash due to the interaction of the tip vortices from the left rotor interacting with the right rotor. These λ_{1c} values will be expected to approach zero as AS approaches infinitely

7. CONCLUDING REMARKS

This work has explored low Reynolds number multirotor aerodynamic interactions for a broad variety of configurations of interest in UAV and drone applications. A coordinated experimental and computational study has been done to uncover and understand important flow interaction phenomena relevant to small size multirotor. The configurations studied in this work were chosen such that the findings are applicable to a large class of multirotor vehicle configurations.
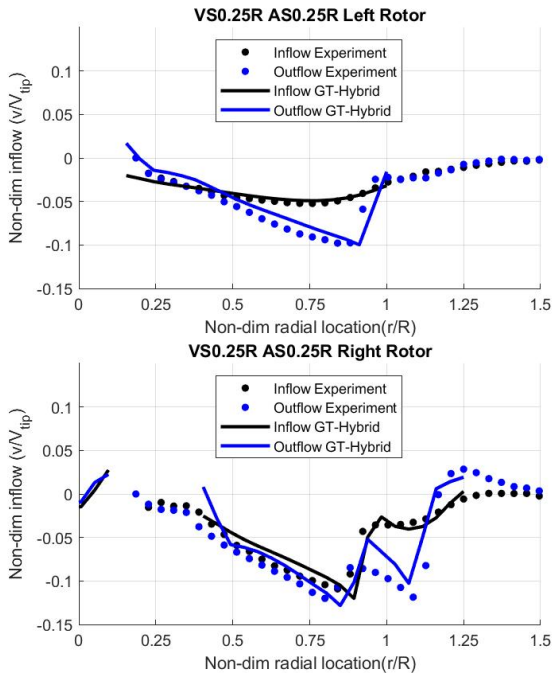
Figure 6. Inflow and outflow velocity profiles comparison for the tandem rotor with VS=0.25R AS=0.25R
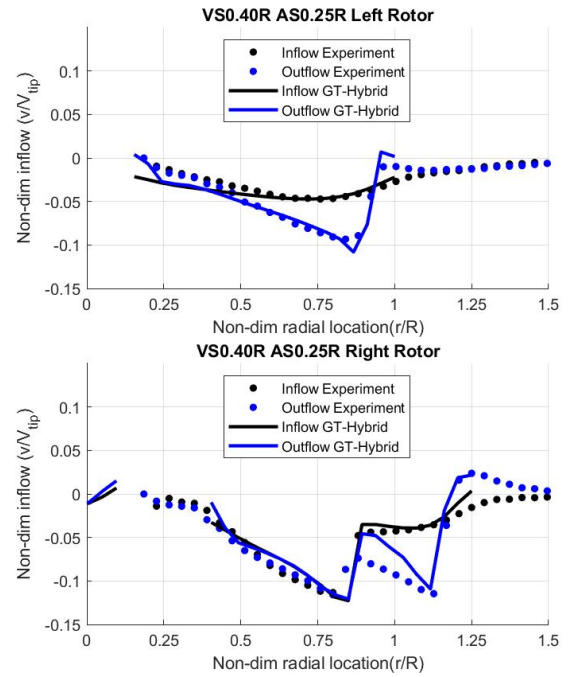

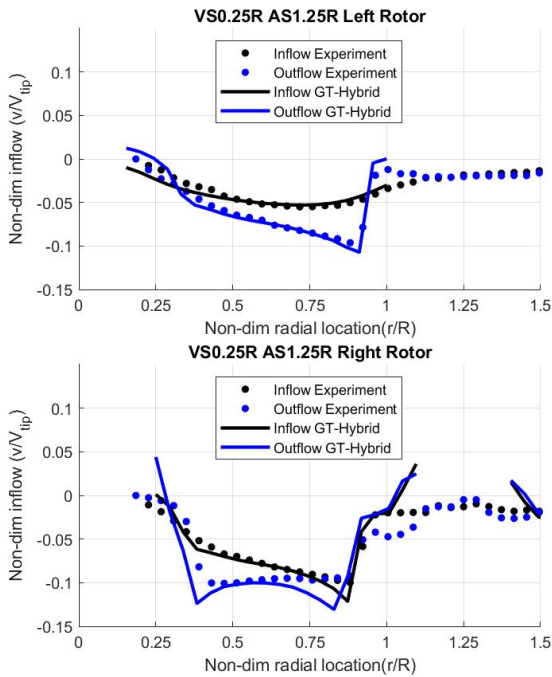Figure 8. Inflow and outflow velocity profiles comparison for the tandem rotor with VS=0.40R AS=0.25R

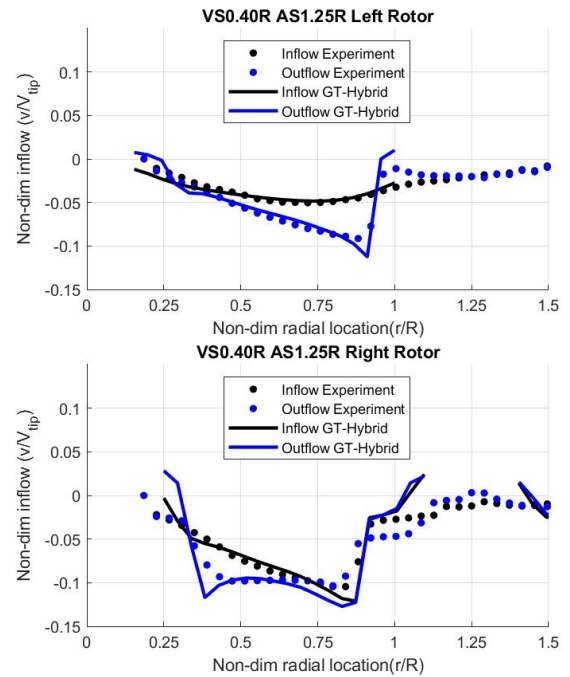Figure 7. Inflow and outflow velocity profiles comparison for the tandem rotor with VS=0.25R AS=1.25R

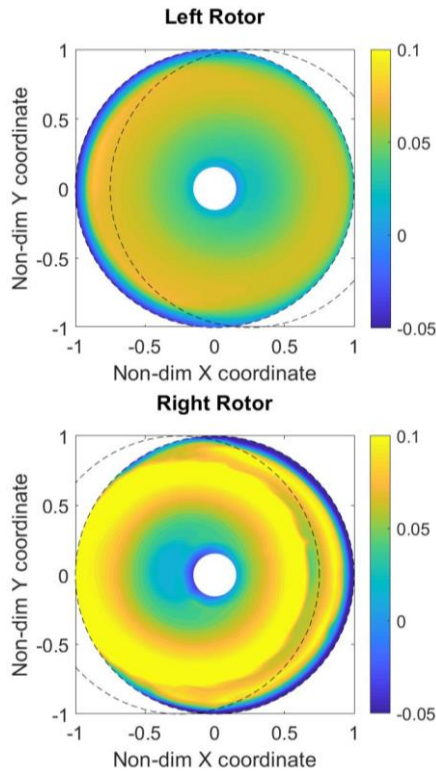Figure 9. Inflow and outflow velocity profiles comparison for the tandem rotor with VS=0.40R AS=1.25R

Figure 10. Induced velocity distribution at the rotor disk for tandem rotor of VS=0.25R AS=0.25R
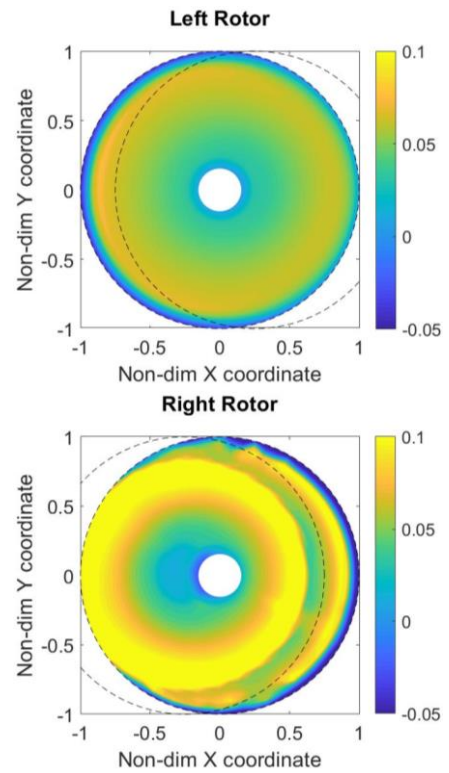
Figure 12. Induced velocity distribution at the rotor disk for tandem rotor of VS=0.40R AS=0.25R
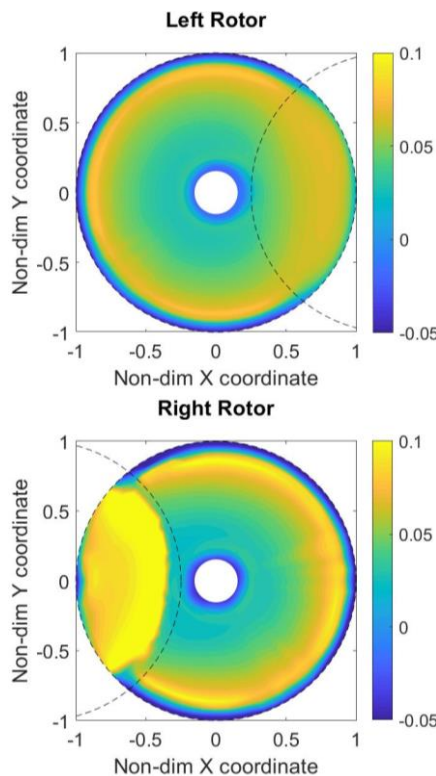
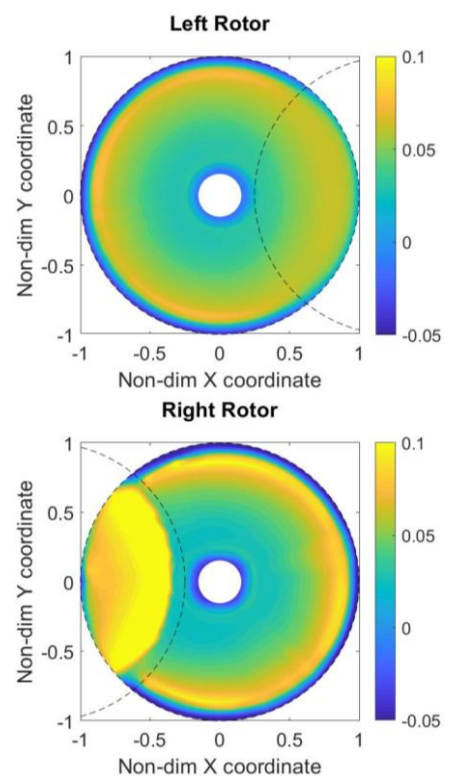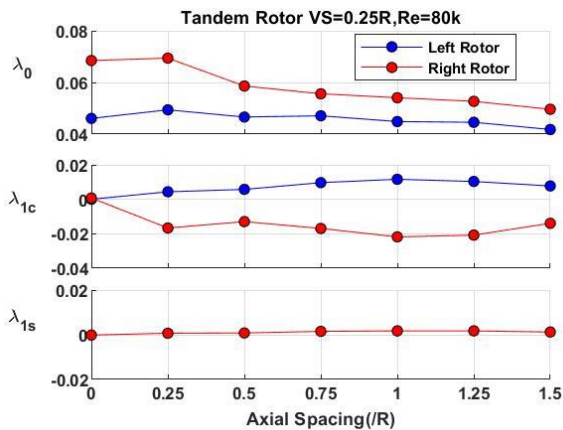Figure 11. Induced velocity distribution at the rotor disk for tandem rotor of VS=0.25R AS=1.25R

Figure 13. Induced velocity distribution at the rotor disk for tandem rotor of VS=0.40R AS=1.25R

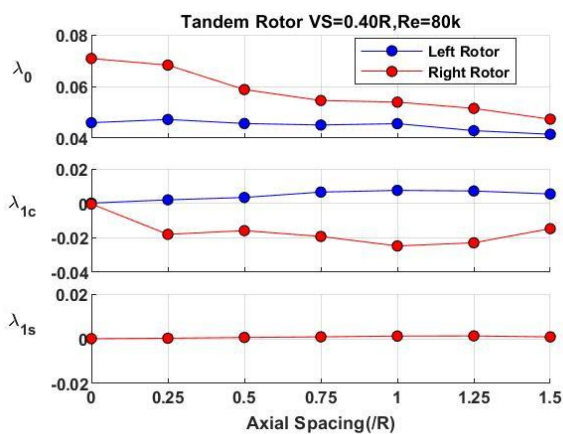Figure 14. Inflow coefficients varies with axial spacing for the tandem rotor with VS=0.25R at Re=80k

Figure 15. Inflow coefficients varies with axial spacing for the tandem rotor with VS=0.40R at Re=80k

The following additional work is in progress. A zero equation transition model is being incorporated into the Spalart-Allmaras model available within the hybrid solver. This would allow larger rotors operating under transition Reynolds number regimes to be modeled properly. Reduced order curve fits for the inflow coefficients λ_0, λ_{1c}, and λ_{1s} are being developed as a function of the rotor thrust, axial, and vertical spacing. Indicial response of the inflow due to step changes to the collective pitch are also being studied.

8. ACKNOWLEDGEMENTS

9. COPYRIGHT STATEMENT

10. REFERENCES

[1] Hariharan, N. S., Egolf, T. A., and Sankar, L. N., "Simulation of rotor in hover: Current state, challenges and standardized evaluation," 52nd Aerospace Sciences Meeting, p. 0041, 2014

[2] Caradonna, F. X. and Tung, C., "Experimental and analytical studies of a model helicopter rotor in hover," NASA TM 81232, 1981.

[3] Lorber, P., Stauter, R., and Landgrebe, A., "A comprehensive hover test of the airloads and airflow of an extensively instrumented model helicopter rotor," 45th Annual Forum of the American Helicopter Society, Boston, MA, 1989

[4] Balch, D. T. and Lombardi, J., "Experimental study of main rotor tip geometry and tail rotor interactions in hover. Volume 1. Text and figures," NASA CR 177336, 1985.

[5] Balch, D. T. and Lombardi, J., "Experimental study of main rotor tip geometry and tail rotor interactions in hover. Volume 2: Run log and tabulated data," NASA CR 177336, 1985.

[6] Marpu, R. P., Sankar, L. N., Egolf, T. A., and Hariharan, N. S., "Simulation of S-76 Rotor in Hover Using a Hybrid Methodology," Proceedings of SciTech 2014, vol. 2014, p. 0210, January, 2014

[7] Rajmohan, N., "Application of hybrid methodology to rotors in steady and maneuvering flight," Ph.D. Dissertation, Georgia Institute of Technology, 2010.

[8] Rajmohan, N., Sankar, L. N., and Costello, M., "Effect of inflow model on coupling between

aeromechanics and flight mechanics," 49th AIAA Aerospace Sciences Meeting, Orlando, FL, 2011

[9] Marpu, R. P., Sankar, L. N., Makinen, S., and Baeder, J. D., "Computational Modeling of Diving-turn Maneuvers using Hybrid Methodology," 68th Annual Forum of the American Helicopter Society, Fort Worth, TX, 2012

[10] Marpu, R. P., Sankar, L. N., Makinen, S. M., Egolf, T. A., Baeder, J. D., and Wasikowski, M., "Physics-based modeling of maneuver loads for rotor and hub design," *Journal of Aircraft,* Vol. 51, (2), pp. 377-389, 2014. doi: 10.2514/1.C031843

[11] Jain, R. K. and Potsdam, M. A., "Hover predictions on the Sikorsky S-76 rotor using Helios," 52nd Aerospace Sciences Meeting, p. 0207, January, 2014

[12] Barakos, G. N., "Evaluating Rotor Tip Shapes Using Computational Fluid Dynamics," Proceedings of SciTech 2014, vol. 2014, p. 0043, National Harbor, MD, January, 2014

[13] Hein, B. R. and Chopra, I., "Hover performance of a micro air vehicle: rotors at low Reynolds number," *Journal of the American Helicopter Society,* Vol. 52, (3), pp. 254-262, 2007. doi: 10.4050/JAHS.52.254

[14] Kunz, P. J. and Stawn, R. C., "Analysis and design of rotors at ultra-low Reynolds numbers," 40th AIAA aerospace sciences meeting & exhibit, p. 99, Reno, NV, 2003

[15] Lakshminarayan, V. K. and Baeder, J. D., "Computational investigation of micro hovering rotor aerodynamics," *Journal of the American Helicopter Society,* Vol. 55, (2), pp. 22001-22001, 2010. doi: 10.4050/JAHS.55.022001

[16] Gupta, V. and Baeder, J. D., "Low Mach number preconditioning for tiltrotor rotor-wing interaction," AHS 4th Decennial Specialist's Conference on Aeromechanics San Francisco, CA, 2004

[17] Schroeder, E. and Baeder, J. D., "Using computational fluid dynamics for micro-Air vehicle airfoil validation and prediction," 23rd AIAA Applied Aerodynamics Conference, p. 4841, Toronto, Ontario, Canada, 2005

[18] Ramasamy, M., "Measurements comparing hover performance of single, coaxial, tandem, and tilt-rotor configurations," 69th Annual Forum of the American Helicopter Society, vol. 31, pp. 21-23, Phoenix, AZ, 2013

[19] Ma, Y., Chen, M., Zhang, X., and Wang, Q., "Scale-model tests of coaxial rotors in water tunnel via particle image velocimetry technique," Proceedings of the Institution of Mechanical Engineers, Part G: Journal of Aerospace Engineering, vol. 230, no. 3, pp. 426-443, 2016

[20] Shukla, D. and Komerath, N. M., "Low Reynolds number multirotor aerodynamic wake interactions," *Experiments in Fluids,* Vol. 60, (4), p. 77, April 2019. doi: 10.1007/s00348-019-2724-3

[21] Shukla, D. and Komerath, N. M., "Drone Scale Coaxial Rotor Aerodynamic Interactions Investigation," *Journal of Fluids Engineering,* Vol. 141, (7), p. 071106, 2019. doi: 10.1115/1.4042162

[22] Shukla, D., "Experimental Study of Low Reynolds Number Multiple rotor Interactions," Ph.D. Dissertation, Aerospac engineering, Georgia Institute of Technology, 2019.

[23] Shukla, D., Hiremath, N., and Komerath, N. M., "Low Reynolds number aerodynamics study on coaxial and quad-rotor," 2018 Applied Aerodynamics Conference, p. 4118, 2018

[24] Chen, P. W., Sankar, L. N., and Prasad, J. V. R., "A Hybrid Navier Stokes - Free Wake Method for Modeling Tandem Rotors," 7th Asian/Australian Rotorcraft Forum, Jeju Island, Korea, October 30 - November 1, 2018

[25] Chen, P. W., Sankar, L. N., Prasad, J. V. R., Schatzman, N., and Rajagopalan, R. G., "Extraction of Dynamic Inflow Models for Coaxial and Tandem Rotors from CFD Simulations," Vertical Flight Society's 75th Annual Forum Philadelphia, PA, May 13-16, 2019

[26] Guner, F., Prasad, J. V. R., Sankar, L. N., Peters, D. A., and He, C., "Correlation of Finite State Multirotor Dynamics Inflow Models with a High Fidelity Viscous Vortex Particle Method," 44th European Rotorcraft Forum, Delft, The Netherlands, September 18-20, 2018